# Inhibition of Human Neutrophil Elastase by $\alpha_1$-Antitrypsin Functionalized Colloidal Microcarriers

**Uta Reibetanz,[†,*] Maria Schönberg,[†] Sophie Rathmann,[†] Vincent Strehlow,[†] Martin Göse,[†] and Jacqueline Leßig[†,‡]**

[†]Institute for Medical Physics and Biophysics, Medical Faculty, University of Leipzig, Härtelstr. 16-18, 04107 Leipzig, Germany, and [‡]School of Materials Science and Engineering, Nanyang Technological University, 50 Nanyang Avenue, 639798 Singapore

**ABSTRACT**

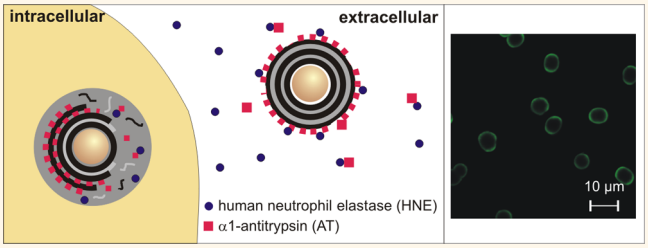


**Layer-by-layer (LbL)-coated microcarriers offer a good opportunity as transport systems for active agents into specific cells and tissues. The assembling of oppositely charged polyelectrolytes enables a modular construction of the carriers and therefore an optimized integration and application of drug molecules. Here, we report the multilayer incorporation and transport of $\alpha_1$-antitrypsin (AT) by colloidal microcarriers. AT is an anti-inflammatory agent and shows inhibitory effects toward its pro-inflammatory antagonist, human neutrophil elastase (HNE). The highly proteolytic enzyme HNE is released by polymorphonuclear leukocytes (PMNs) during inflammatory processes and can cause host tissue destruction and pain. The high potential of this study is based on a simultaneous intra- and extracellular application of AT-functionalized LbL carriers. Carrier application in PMNs results in significant HNE inhibition within 21 h. Microcarriers phagocytosed by PMNs were time dependently decomposed inside phagolysosomes, which enables the step-by-step release of AT. Here, AT inactivates HNE before being released, which avoids a further HNE concentration increase in the extracellular space and, subsequently, reduces the risk of further tissue destruction. Additionally, AT surface-functionalized microcarriers allow the inhibition of already released HNE in the extracellular space. Finally, this study demonstrates the successful application of LbL carriers for a concurrent extra- and intracellular HNE inhibition aiming the rebalancing of protease and antiprotease concentrations and the subsequent termination of chronic inflammations.**

**KEYWORDS:** LbL carriers · biocompatible polyelectrolytes · chronic inflammation · drug delivery · $\alpha_1$-antitrypsin · polymorphonuclear leukocytes · human neutrophil elastase

Many diseases of civilization are accompanied by chronic inflammations resulting in tissue destruction and pain. Current medication has several drawbacks due to the systemic application. On the one hand, high doses are needed to overcome the transport-related loss of agents and their activity reduction. As a consequence, high doses can result in severe side effects. Glucocorticoids, immunosuppressants, and nonsteroidal antirheumatic agents lead to impairment of immune system, blood, liver, and kidney and an increasing risk of infections.[1,2] On the other hand, a local as well as sustained drug release is not possible but would be the basis for a gentle and side-effect-less treatment. Thus, there is a high demand for an up-to-date medical treatment. The direct transport and delivery of low amounts of active agents into inflamed tissues and immune stimulatory cells is a promising approach to overcome these current problems.

Layer-by-layer (LbL)-coated, functionalized colloidal microcarriers can be used as local transporters of highly specific anti-inflammatory substances. In general, the design of such carriers is based on spherical templates with various sizes.[3] The LbL coating is performed by means of oppositely charged biopolyelectrolytes allowing the formation of hollow capsules by core dissolution.[4] The advantages are clearly defined in a high multifunctionality. The multilayers, hollow capsules, or porous templates provide transport capacities for several active agents such as peptides, nucleic acids, antigens, enzymes,[5−9] or reporter molecules such as pH-sensitive molecules or encoded DNA[10−13] either alone or combined[14,15] in one system.

The uptake and subsequent release within specific cell compartments is widely investigated *in vitro*. The latter can be intracellularly caused by multilayer widening or degradation[16−19] due to specific intracellular conditions and stimulation, whereas specific cell internal conditions (pH, glucose sensitivity,[20,21] or external parameters (laser, ultrasonic exciation[22−24]) can serve as triggers. Additionally, specific surface functionalizations can be applied to facilitate an accelerated (*e.g.*, by cell-penetrating peptides as surface functionalization[25]) or specific cell uptake (*e.g.*, by antibodies against cancer cells[26]),

* Address correspondence to uta.reibetanz@medizin.uni-leipzig.de.

Received for review April 24, 2012 and accepted June 17, 2012.

**Published online June 18, 2012**
10.1021/nn301791w

making the system even more interesting for highly specialized drug delivery.

Thus, using the modularity of the system by combining those features, the approach provides the opportunity of a controlled and highly specific drug application and can be designed to bypass problems occurring during systemic drug release, which demonstrates a very promising therapy concept.

Recently, *in vivo* studies observed the processing and efficacy of functionalized microcarriers in tissue. After subcutaneous injection and uptake, LbL capsules demonstrated only a moderate immune reaction,[27] which strongly supports the applicability as medical carriers. Vaccination studies in mice were validated in murine influenza as well as melanoma models.[9]

However, several challenges such as transport to the desired tissue or early multilayer degradation in extracellular space and phagolysosomes have to be considered for the general application of LbL microcarriers as a drug delivery system. Hence, in our approach, the specific LbL carrier application for inflammatory treatment strongly benefits from a direct application into locally inflamed tissue to transport and release the anti-inflammatory $\alpha_1$-antitrypsin (AT) into phagolysosomes of polymorphonuclear leukocytes (PMNs) in addition to the extracellular use.

Although PMNs play an important role as the first defense of the immune system, a massive invasion into tissues can lead to deleterious chronic inflammation. Stimulation-mediated release of highly degradative substances such as proteases, hydrolases, peroxidases, as well as reactive oxygen species[28−30] from lysosomes and azurophilic granules causes pro-inflammatory macrophage signaling and contributes to the manifestation of the chronic process.[29] The focus of this study is the inhibition of a principal degradative enzyme, human neutrophil elastase (HNE), from its source, the PMNs.

Here, AT is transported as a constituent of biocompatible and biodegradable multilayers assembled on colloidal microcarriers ($5 \pm 1$ $\mu$m). The advantage of this design is the transport of a low but well-defined amount of antiprotease combined with a consistent release rate due to a gradual multilayer decomposition. Two general obstacles of carrier-based drug delivery systems will be avoided especially regarding the inhibition of intracellular HNE of PMNs. First, the application of carriers can be carried out subcutaneously, directly into confined inflamed loci (such as in rheumatoid arthritic tissue), avoiding the bloodstream transport and, therefore, an early clearance of the carriers. Second, PMN phagolysosomes constitute the intracellular target compartment. Although the detailed uptake mechanism and time scales are not yet fully understood,[31] it can be presumed that carriers will be phagocytosed and eventually end up in the phagolysosomes. In our application, the challenging carrier escape into cytoplasm, the target location of most active agents, is not required. After uptake and phagolysosomal/granular fusion, the carriers are exposed to the highly active lysosomal compounds including multilayer decomposing enzymes and target HNE. Thus, the combined HNE inhibition at its place of origin and additionally at the extracellular space by nonphagocytosed carriers is the main advantage of this approach and an absolute novelty.

Nevertheless, several questions arise from this application: Is it possible to integrate a sufficient amount of AT within different layer depths of a multilayer with full activity, and is the multilayer stable under storage conditions? After microcarrier phagocytosis and the subsequent enzymatic layer decomposition, is there AT degradation or can we obtain HNE inhibition within the short PMN's lifetime? Our own studies with protamine sulfate (PRM)/dextran sulfate (DXS)-coated $CaCO_3$ microparticles are promising as they show multilayer decomposition within HEK 293T/17 cells,[10] as well as after incubation with the supernatant of stimulated and lysed macrophage-like U937 cells[32] and PMNs.[33]

Here, specific AT-functionalized carriers were investigated regarding their inhibitory effect toward pure HNE in supernatants of stimulated PMNs containing HNE as well as to PMNs in a time-dependent and cell/carrier ratio-dependent study. The successful HNE inhibition by means of these AT-functionalized carriers highlights the potential of a microcarrier application in inflamed tissue.

## RESULTS AND DISCUSSION

**AT Assembling as Multilayer Constituents.** In our investigations, we used PRM and DXS to build up the multilayers. Those polyelectrolytes are known to be biocompatible as well as biodegradable within several cell compartments, causing the subsequent release of the transported agents.[10,33] For the optimization of the coating conditions, AT was labeled with FITC. Using a FITC antibody labeling kit, a label degree of $0.24 \pm 0.02$ could be obtained. Figure 1 shows the assembling of AT onto the PRM/DXS multilayers coated on $CaCO_3$ microcarriers. In our investigations, AT was assembled as a negatively charged layer in different layer positions. With an isoelectric point between 4.9 and 5.3,[34] AT was coated in buffers ranging from pH 7 to 9. Best coating conditions were found using borate buffer at pH 8.5/0.5 M NaCl solution. This coating strategy was used, although a possible loss of the weakly charged protein during the assembly of the next regular polyelectrolyte layer may occur as addressed in Temmerman *et al.*[35] Here, protein-loaded $CaCO_3$ cores show a loss of protein from the core's surface after coating the first DXS layer, probably caused by competition processes. Also, exchange processes of PRM in the interaction with the multilayer material may influence the assembly.[36] Nevertheless, the alternative assembly of protein−polymer complexes would most likely result

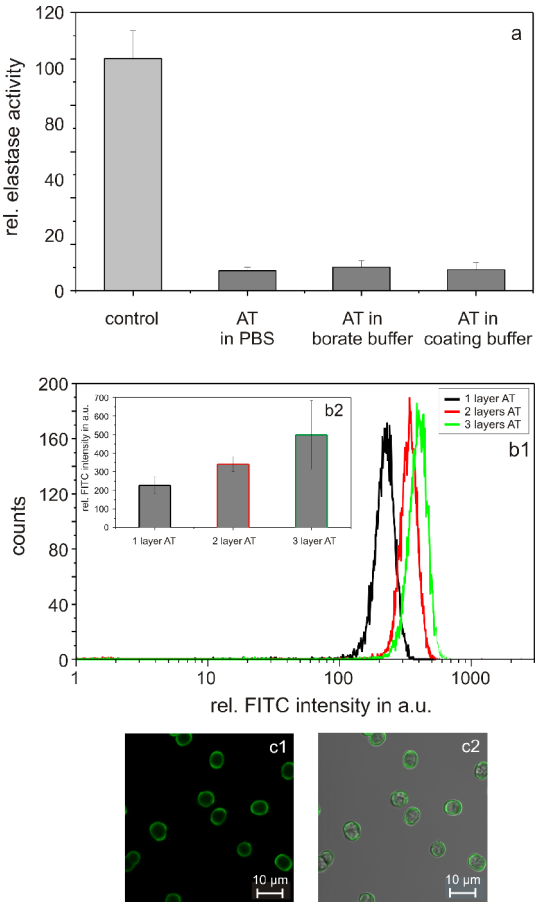


**Figure 1. AT assembling as PRM/DXS multilayer constituent. (a) Photometric investigations of relative HNE activity are shown regarding the influence of coating buffer on AT activity; 68 nM HNE was exposed to 0.5 $\mu$M AT in different buffers (buffer for model experiments, storage buffer, coating buffer) as well as 1 mM specific substrate. Control was HNE/substrate solution without AT, which was set to 100%. (b1,b2) FCM measurements of AT-FITC adsorption in different layer depth are shown. Representative FITC intensity distributions of single carriers are shown in (b1), whereas the black curve marks one layer AT, the red curve two layers, and the green curve three layers AT following the coating scheme $CaCO_3$|PRM/DXS/PRM/DXS/PRM/AT/PRM/AT/PRM/AT. The intensity distribution in (b2) illustrates the linear increase in FITC fluorescence intensity with increasing AT layer number. The CLSM images in (c) illustrates the successful coating of FITC-labeled AT onto the PRM/DXS multilayers, comparing fluorescence image (c1) and its overlay with transmission image.**

in a strong AT activity reduction as already shown for enzyme–polymer complexes as multilayer constituents, whereas an enhanced aggregation status of the enzyme was discussed causing loss of activity.[37] Additionally, all buffers used in the experiments did not influence the activity of immobilized AT (Figure 1a): 0.5 $\mu$M AT in PBS (control experiments), in borate buffer (AT dissolution and storage buffer), and in borate buffer/0.5 M NaCl solution (coating buffer) exhibits the same inhibitory activities toward 68 nM HNE.

In Figure 1b, the coating of several AT layers is presented according to FCM analysis. For drug delivery systems, it may be important to integrate active agents into different layer depths, as there are several advantages. First, the agent is protected from degradation by reactive molecules in biological environments.[10] Second, the step-by-step integration into the multilayers provides an assembly of several different agents[38] without interference as well as a sequential decomposition within the desired cell compartment, facilitating a sustained release.[39] Figure 1b1 shows an example of a FCM histogram of single carriers. The black, red, and green intensity distributions correlate with carriers equipped with one, two, and three layers of AT, respectively. The inset (Figure 1b2) represents the geometric mean of the intensity data of three preparations, indicating a linear intensity increase and, therefore, a linear increase in AT coating. On the basis of the label degree of each AT molecule and FCM measurements of FITC-labeled calibration beads, the AT amount building up one layer can be estimated as 5 $\pm$ 2 pg.

Figure 1c demonstrates the homogeneous distribution of AT as a multilayer constituent, presented in the CLSM image of FITC distribution (Figure 1c1) and an overlay of FITC intensity and transmission images (Figure 1c2), both illustrating one outermost AT layer of the PRM/DXS multilayer.

**Stability of AT Layers.** For medical applications, AT layers have to be stable under storage conditions but should be releasable in biomedically significant regions or cell compartments. To investigate carrier stability within various environments, carriers coated with one, two, and three AT-FITC layers were incubated in 0.1 M NaCl solution and full medium. Afterward, fluorescence intensities of the carriers were time dependently investigated with FCM related to the different AT coating schemes and compared to carrier control investigations carried out immediately after preparation. Figure 2 shows the FITC intensities depending on the AT layer number. Layer 6 indicates one AT layer, layer 8 refers to two AT layers, and layer 10 marks the presence of three labeled AT layers.

The carriers were incubated up to 48 h in 0.1 M NaCl as well as 24 h in 0.1 M NaCl followed by 4 or 24 h in DMEM with 5% FBS, respectively. As can be seen, the fluorescence intensities vary depending on medium and incubation time.

The different incubation conditions were chosen according to the different conditions in cell experiments. The combination of NaCl solution and full medium refers to storage conditions followed by cell application. A 4 h incubation in DMEM/5% FBS marks carrier uptake by PMNs since the uptake is supposed to be nearly complete after that incubation time.[33] The literature provides a wide time interval for the PMN life span, differing from a half-life of 6 h[40] to 24–48 h[29] circulating in blood, as well as an extension of the PMN life span described in inflamed tissue. In this study, 21–24 h as a maximum interval for incubation experiments with carriers is applied. This interval describes the mean

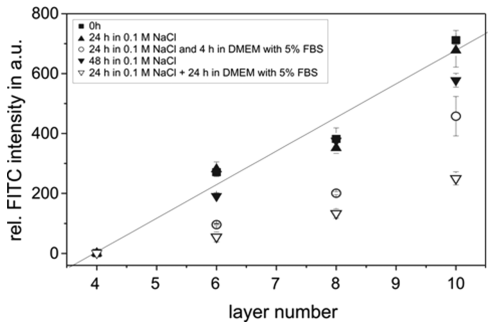


**Figure 2. Stability of the AT coating on the microcarrier. FITC-labeled AT was used to build up one (layer 6), two (layer 6, 8), or three layers (layer 6, 8, 10) as constituents of the PRM/DXS multilayer according to the coating scheme in Figure 1. FITC intensity was detected by FCM. The graph shows the dependence of fluorescence intensity and, therefore, of the layer amount of AT at various storage conditions. As reference, 0.1 M NaCl storage solution and an incubation time frame up to 48 h were used. Twenty-four hour carrier incubation with 0.1 M NaCl followed by 4 h in DMEM with 5% FBS (full medium) illustrates combined storage and cell conditions, where a cell/carrier interaction and uptake time frame of maximal 4 h was considered. A 24 h, storage in full medium symbolizes the entire cell/carrier interaction time frame considering the PMN lifetime with good vitality.**

lifetime of PMNs at good vitality (15% necrotic cells[41]) and, therefore, the most probable period of an effective application. As reference, 24 or 48 h storage in NaCl solution indicates storage conditions. Here, after 24 h, no changes in fluorescence intensity could be observed, indicating a full stability of the AT layers. After 48 h, a moderate decrease was detectable.

During the exposition of AT-functionalized microcarriers to full medium, the fluorescence intensity and, consequentially, the AT amount as multilayer constituents significantly decreased. Microcarriers with only one outermost AT layer (layer 6) experience an AT reduction to about 50 ± 2% (4 h) and 29 ± 9% (24 h), respectively, in the presence of interacting polyelectrolytes as proteins. With the coating of two or three layers, the AT loss becomes more pronounced (layers 6, 8 and layers 6, 8, 10). After 4 h, the intensity is reduced to 57 ± 2% and 67 ± 10%, respectively. After 24 h, a reduction to 38 ± 5% and 37 ± 3% can be observed. That means, for example, in the case of three layers of AT, an intensity loss of about 1/3 (4 h) and 2/3 (24 h) is correlated to the loss of one layer and two layers of AT, respectively. Compared to the previous design (one layer AT), it can be assumed that an irregular, unsequential multilayer decomposition takes place since here even after 24 h a considerable amount of AT is immobilized at the carrier surface. Considering the fact that AT has to contribute to both extracellular and intracellular HNE inhibition, AT release from the outermost microcarrier layers by means of polyelectrolyte interaction may contribute to the inhibition of already released HNE in the extracellular space. Meanwhile, still immobilized AT of the inner layers is assumed to be effective in an intracellular way.

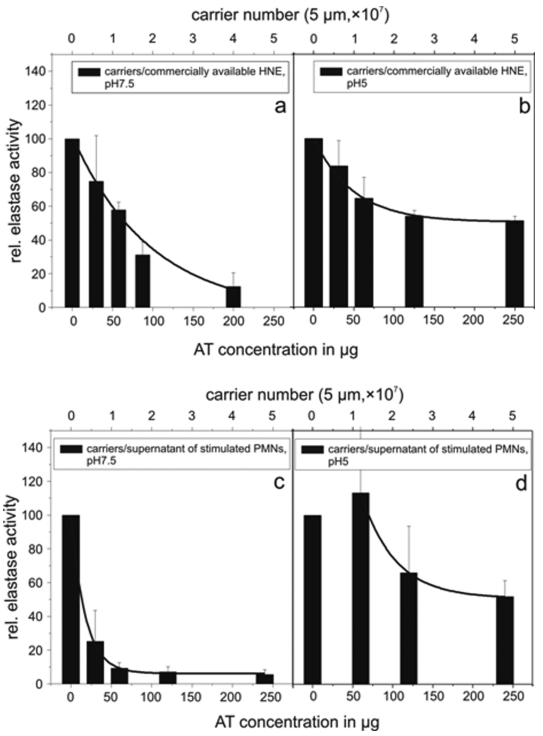


**Figure 3. (a,b) Interaction of different AT carrier numbers with commercially available HNE at pH 7.5 and 5, respectively. HNE activity was detected photometrically after incubation with specific substrate; 0.2 $\mu$g of HNE (68 nM) was used according to the HNE content of 3 × $10^5$ cells. In comparison, (c,d) show investigations with AT carriers incubated with the supernatant of 3 × $10^5$ stimulated PMNs. As reference value, HNE activity without AT treatment was set to 100%. The carrier number was also transcribed as the calculated total amount of AT assembled as an outermost layer (upper and lower *x*-axis).**

Besides AT stability in the layers, the AT activity as a multilayer constituent has to be considered, too. Therefore, the next investigations are focused on inhibitory capability regarding HNE.

**Short-Time AT Carrier Interaction with Commercially Available HNE and with the Supernatant of Stimulated PMNs.** According to previous findings in experiments using free (unimmobilized) AT,[42] HNE inhibition is relatively rapid. To investigate the inhibitory activity of immobilized AT, carriers with one outermost AT layer were incubated with defined concentrations of commercially available HNE as well as with the supernatant of stimulated PMNs for 5 min, and HNE activity was determined after substrate addition.

Figure 3 shows the investigations at different pH values. The experiment illustrates the interaction of AT with HNE released into the extracellular space at about neutral/slightly acidic pH of inflammatory tissues as well as at pH 5 symbolizing the late phagolysosome/granule.[43] According to Schönberg *et al.*,[42] there is no difference in AT activity toward HNE inhibition between pH 7.5 and 7.0. Therefore, the experiment simulating extracellular conditions was performed at pH 7.4.

Thus, Figure 3a,b represents the interaction of different AT carrier numbers with commercially available HNE at pH 7.4 and 5, respectively. Here, 0.2 $\mu$g of HNE (68 nM) was used according to the HNE content of $3 \times 10^5$ cells.[44] In comparison, Figure 3c,d shows investigations with AT carriers incubated with the supernatant of $3 \times 10^5$ stimulated PMNs. All graphs present the relative HNE activity after the application of different AT carrier concentrations. As a reference value, HNE activity without AT treatment was set to 100%. Additionally, the carrier number was transcribed as the calculated total amount of AT assembled as the outermost layer (upper and lower *x*-axis).

In all investigations, the relative HNE activity decreases with increasing carrier amount, but the curve progressions differ depending on pH and HNE source.

Using commercially available HNE and AT, at pH 7.4, a calculated cell/carrier ratio of 1:40 ($120 \times 10^5$ carriers, $3 \times 10^5$ cells) is required for a 50% HNE inhibition (Figure 3a). Considering the conditions of the late phagolysosome characterized by an acidic pH (around pH 5), the situation becomes more challenging regarding the AT activity maintenance within drug carriers (Figure 3b). Here, a cell/carrier ratio of 1:160 is necessary for 50% HNE inhibition. The pH-dependent activity changes,[42,45,46] and partial polymerization of immobilized AT[47,48] and the reduced model environment compared to cells may influence the inhibitory efficiency of AT. This condition would demand a very high carrier amount in order to inhibit HNE inside the phagolysosomal compartment. In the case of applying AT to the supernatant of stimulated PMNs at pH 7.4 (Figure 3c), the effective cell/carrier ratio is considerably better. Only 8 carriers per cell could be found effective, inducing a 50% HNE inhibition. These findings of an enhanced inhibitory effect in PMN supernatant are in good agreement with Schönberg *et al.*,[42] indicating the efficacy of additionally existing HNE inhibiting substances. Nevertheless, at pH 5, a similar result can be obtained, as already shown for carrier application to commercially available HNE at pH 5, making a cell/carrier ratio of 1:160 necessary to produce a 50% HNE inhibition.

In parallel, all cell/carrier experiments were also compared to HNE activity measurements using free AT under consideration of the same pH and environmental conditions as shown above (data not shown). The comparison of inhibitory abilities of free and carrier-immobilized AT illustrates a restricted efficacy of immobilized AT of about 10%. We propose that, due to assembling as a negatively charged layer and electrostatic interaction with the previously adsorbed, positively charged PRM layer, the reactive center of AT may, in this case, not be sufficiently accessible to HNE to initialize a successful 1:1 enzyme−inhibitor complex formation.[49]

These results illustrate that the short-time application of AT-functionalized carriers, which means still immobilized AT, does not lead to a sufficient HNE inhibition, neither under acidic nor under neutral conditions. The number of AT carriers causing a 50% HNE inhibition is proved to be too high for medical treatment, even if the cells would be able to internalize such a high amount of carriers. As a consequence, it can be assumed that AT has to be released from the carrier multilayers to be effective, which may occur after a long-time application and under specific extracellular or phagolysosomal conditions. Here, degradation of the multilayers and the subsequent AT release triggered by proteins and lysosomal enzymes has not yet proceeded. Additionally, microcarriers are not only interacting with PMNs, as they will be also incorporated by other phagocytosing cells as macrophages. As key players in inflammatory tissues, they are responsible for the clearance of necrotic cellular material and subsequently, by means of cytokine signaling, for the fate of inflammatory processes.[40] Therefore, it has to be ensured that microcarriers by themselves are not contributing to pro-inflammatory signaling, which urgently suggests a low carrier number application. In previous investigations, it was shown that a low cell/carrier ratio (up to 1:5) resulted in only marginal pro-inflammatory response (low TNF$\alpha$ and IL1$\beta$ release).[32] A low cell/carrier ratio as well as biocompatible and biodegradable carrier materials is therefore of high importance for the treatment of inflamed tissue.

In summary, a defined number of carriers transporting a defined amount of AT seem to be necessary for efficient treatment, taking advantage of degradation effects causing AT release for better inhibitory effects, which is outlined in the next investigations.

**AT Carrier/PMN Interaction within PMN's Life Span.** A 21 h application of AT carriers in PMNs causes a different effect. In order to apply drug-loaded microcarriers for the treatment of chronic processes, the administration time can be extended toward PMN life span. Since a good PMN viability (85% non-necrotic cells) was shown up to 24 h after isolation from human blood,[41] this study of HNE inhibition after carrier uptake and processing was extended according to this PMN life span. This allows the identification of the AT carrier potential as an effective drug delivery system.

In this time span, three possible processes can occur: (1) Carriers will be taken up and processed by PMNs (phagolysosomal pH 5). (2) They will remain within the extracellular space (pH 7.4 and below) or attached to the cell surface to be processed by protein interaction and extracellular degradative substances which are released by stimulated cells.[45] (3) Carriers will be phagocytosed and cleared by macrophages. The following investigations are focused on exclusive PMN/carrier interaction summarizing the processes of the first two points.

AT surface-functionalized carriers (transporting $5 \pm 2$ pg of AT) were coincubated with PMNs for 5 and 21 h.

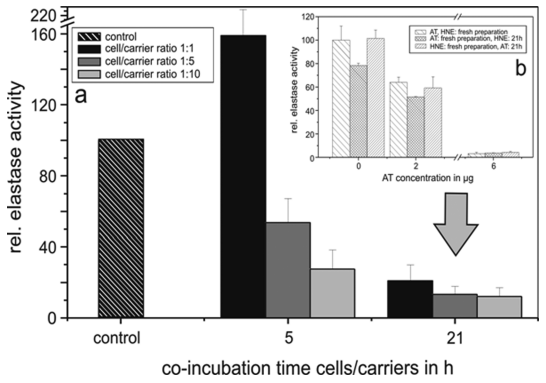


**Figure 4. (a) Photometrical investigations of HNE activity after incubation of AT carriers with PMNs in different ratios. AT was assembled as the outermost layer onto 5 layers of PRM and DXS. After 5 and 21 h co-incubation, supernatant was collected and exposed to specific substrate. PMNs without carrier treatment serve as control, and HNE activity was set to 100%; results of cell/carrier co-incubation were presented in relation to the control. Cell/carrier ratios of 1:1, 1:5, and 1:10 were used according to previous finding, providing good cell viability.[19] (b, Inset) HNE and AT activity progressions are shown depending on the storage time of each substance in reaction buffer. Here, HNE activity of freshly used AT and HNE (left bars) was compared to 21 h stored HNE/freshly used AT (middle bars) and 21 h stored AT/freshly used HNE (right bars).**

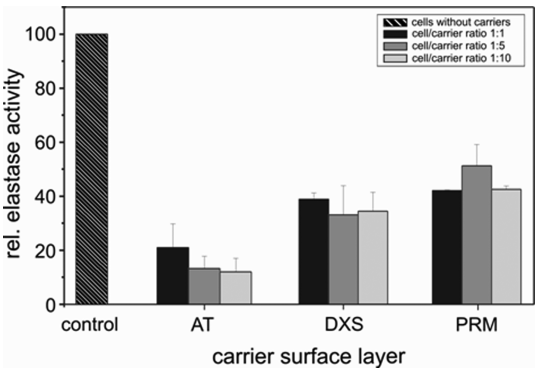


**Figure 5. Photometric investigations of HNE activity after incubation with nonfunctionalized (PRM or DXS as surface layer) and AT-functionalized carriers with PMNs in different ratios. As a control, supernatant of PMNs without carrier treatment and AT surface-functionalized carriers were used (striped bar). HNE activity of PMNs without carrier treatment was set as 100%, and all results were presented in relation to the control. The cells were co-incubated with carriers for 21 h, which is expected to be the longest possible time frame with good PMN viability.**

According to Rathmann *et al.*,[33] cellular attachment and uptake take place within the first 2−4 h followed by the phagolysosomal decomposition of up to five layers of PRM/DXS. Thus, it can be expected that an intracellular release of immobilized AT may occur during the remaining 20−22 h, according to the approximated lifetime of 24 h.[29] This process is accompanied by extracellularly occurring AT release from the remaining carriers due to their interaction with concomitantly released enzymes from constantly stimulated cells. This release is caused by continuing cell stimulation due to carrier presence as well as the $Ca^{2+}$-containing $HBSS^{+}$ buffer conditions.

For co-incubation experiments, cell/carrier ratios of 1:1, 1:5, and 1:10 were adjusted according to Lessig *et al.*[32] In Figure 4a, HNE activity was photometrically determined after time-dependent carrier treatment and subsequent PMN stimulation. Cells without carrier treatment were used as control, and their resulting HNE activity depending on the experimental time span was set to 100%.

With increasing cell/carrier ratio, 1:5 and 1:10, HNE activity is significantly reduced after 5 h to 53.6 ± 13.5 and 27.6 ± 10.7%, respectively. Also, the increased co-incubation time (21 h) results in a more pronounced HNE inhibition. Here, only 20.9 ± 8.8, 13.2 ± 4.6, and 12.0 ± 4.9% HNE activity could be found after the cell/carrier application of 1:1, 1:5, and 1:10, respectively. Interestingly, the differences are now marginal, and the application of 1:5 and 1:10 shows nearly the same results. The experiments show, in comparison to short-time incubation, that after long-time application even a low dose is sufficient to produce a considerable effect, which is in good agreement with biocompatibility investigations.[32]

Two other aspects have to be considered. (1) A HNE activity loss may take place during the 21 h experiment. Thus, control experiments were carried out and are demonstrated in Figure 4b. Here, different AT ratios were chosen and co-incubated with commercially available HNE. HNE activity was measured after co-incubation with a specific substrate. Compared to the control using fresh AT and HNE (left bar, full HNE activity without AT treatment was set to 100%), HNE and AT were stored for 21 h under 37 °C and then exposed to freshly prepared AT (middle bar) and HNE (right bar), respectively. In all cases, AT storage seems not to impair its activity, but a 21 h storage of HNE reduces its activity to about 80%. With increasing AT concentrations, the HNE activity reduction becomes less pronounced. At low AT concentrations (2 $\mu$g, according to a cell/carrier ratio of about 1:1), the HNE activity is reduced to about 85%, whereas at higher AT concentrations (6 $\mu$g and more, according to a cell/carrier ratio of about 1:5), the inhibiting effect on HNE is dominant. (2) Interestingly, the HNE activity-reducing effect is not exclusively caused by AT. In Figure 5, co-incubation experiments of AT carriers with PMNs in comparison with unfunctionalized carriers are shown. Here, a 21 h co-incubation with microcarriers coated with 5 layers of PRM/DXS and an outermost PRM layer (layer 5) as well as outermost AT or DXS layers (layer 6) was performed. Photometric investigations of HNE activity are shown after cell/carrier co-incubation using rates of 1:1, 1:5, and 1:10. As a control, cells were seeded into the wells without carrier treatment for 21 h, HNE activity was set as 100%, and all measurements were presented in relation to the control.

The application of PRM or DXS surface coated carriers to PMNs results into two findings. At first,

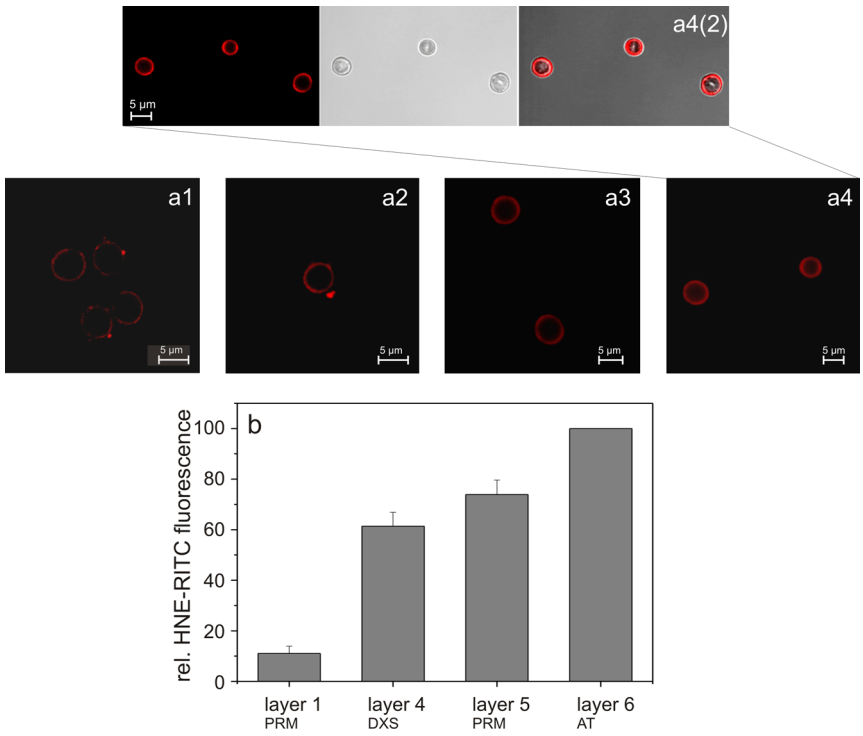


**Figure 6. FCM and CLSM investigations of the HNE interaction with polyelectrolyte-coated microcarrier surface. HNE was labeled with NHS-Rhodamine and incubated with $10^6$ microcarriers for 2 h in 100 $\mu$L of PBS. (a) CLSM images of HNE adsorption. (a1) HNE binding to carriers with only one PRM layer, (a2) to carriers with 4 layers PRM/DXS with DXS as the outermost layer, (a3) to carriers with 5 layers PRM/DXS with PRM as the outermost layer, and (a4) to carriers with 5 layers PRM/DXS followed by AT as the outermost layer. To show the correlation between core and multilayer, a4(2) illustrates the circular appearance of HNE on $CaCO_3$ templates as the transmission image and overlay example for AT carriers. Quantitative investigations of fluorescence intensity by FCM are shown in (b).**

a HNE inhibition within PMNs can be detected, as well, although there seems to be no ratio dependency. However, in relation to AT carriers, the unspecific inhibitory effect of biopolymer-coated carriers causes only a reduction of HNE activity to about 40%. The specific inhibitory effect of AT can be estimated up to 20−30% using cell/carrier ratios of 1:5 and 1:10, respectively.

HNE inhibition studies of Schönberg *et al.*, using the supernatant of stimulated PMNs,[42] demonstrate a 20−30% HNE activity reduction after application of 0.2 $\mu$M AT (1.05 $\mu$g) per $3 \times 10^5$ cells at acidic conditions. In our investigations, this effect will be achieved using only one outermost AT layer (about 5 pg AT/carrier, Figure 1) and a 1:5 cell/carrier ratio, that is, 7.5 $\mu$g of AT/$3 \times 10^5$ carriers. Considering a possible 50% loss of immobilized AT during extracellular degradation before uptake (as shown in Figure 2) and only a gradual release of AT from the carriers, the same effect can be obtained using 3 times the amount of freely available AT. Second, the inhibitory effect of the multilayer polyelectrolytes seems to be independent of the charge of the molecule. PRM and DXS, assembled as the surface layer, are causing the same unspecific effect toward HNE.

The polyelectrolyte-mediated HNE inhibition indicates either an immobilization of HNE onto the charged surface of the multilayers parallel to an irregular multilayer decomposition or an intercalation into the core after the penetration of the multilayers or HNE complexation with already released PRM and DXS. Investigations regarding the nature of the unspecific HNE immobilization on the remaining carrier surface are shown in Figure 6. Here, NHS-Rhodamine-labeled HNE was incubated with microcarriers in different states of coating for 2 h. In line a (a1−a4), CLSM investigations are shown to detect potential HNE binding toward different surface polyelectrolytes: a1 shows the HNE interaction with a one-layer coated microcarrier (PRM), symbolizing an advanced multilayer decomposition. Panels a2−a4 show the HNE interaction with negatively charged DXS as layer 4, positively charged PRM as layer 5, and AT as layer 6. Figure 6a4(2) (AT as layer 6) clearly illustrates the circular HNE distribution around the $CaCO_3$ template by comparing the fluorescence image, transmission image, and their overlay. In Figure 6b, FCM investigations are illustrating the quantitative analysis of fluorescence intensities.

Figure 6a1 shows weak, non-homogeneous red circular appearance around the core. Staining of the core could not be observed. The low fluorescence intensity can also be verified by FCM analysis (Figure 6b).

In contrast, in Figure 6a2−a4, an increased interaction of HNE with the multilayer material can be observed. The CLSM images show a bright fluorescence and homogeneous HNE distribution around the multilayers.

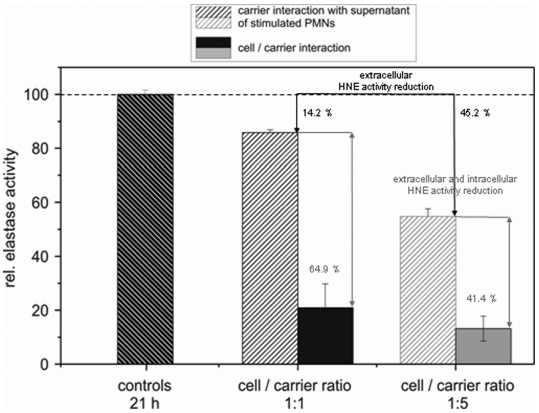


**Figure 7. Photometrical investigations of HNE activity after 21 h incubation of AT carriers with supernatant of stimulated PMNs (striped bars) compared to cell/carrier interaction (filled bars). Cell/carrier ratios of 1:1 and 1:5 were used. As reference, supernatant of stimulated cells as well as PMNs without carrier treatment (both after 21 h) were set as 100% (striped bar), and all cell/carrier results were presented in relation to the control.**

In Figure 6b, a strong increase in fluorescence intensity can be observed, as well. AT as the surface layer shows stronger HNE binding due to specific interactions. PRM and DXS, on the other hand, represent comparable binding abilities. Since HNE has an isoelectric point at about 10−11,[50] it is predominantly positively charged at pH 5 or 7.5, respectively. Therefore, it can easily interact with negatively charged DXS as the outermost layer. In contrast to the 70 kDa DXS, PRM was characterized by a low molecular weight of about 4200 Da, which is probably not covering the entire DXS surface sufficiently, hence partly leaving negatively charged DXS exposed. Here, an interaction of PRM with HNE can take place explaining the HNE binding at an outermost PRM layer.

These results are in good agreement with the photometrically detected HNE activity loss after 21 h PMN/carrier co-incubation (Figure 5) and suggest a partial contribution of the HNE immobilization to the subsequent HNE inactivation/activity reduction.

**Differentiation between Extra- and Intracellular HNE Inhibition.** It is now interesting to demonstrate the advantage of the HNE inhibitory effect of AT microcarriers on the entire cell system (intracellular as well as extracellular effect) compared to the effect of exclusively extracellularly effective carriers (Figure 7).

In parallel to cell/carrier co-incubation experiments known from Figure 4 (shown as filled bars in Figure 7), the experimental setup was modified. PMNs were stimulated immediately after isolation, and supernatant was collected for microcarrier incubation. For all experiments, co-incubation was performed for 21 h and low cell/carrier ratios of 1:1 and 1:5 were applied (black-striped bar indicating a cell/carrier ratio of 1:1, gray-striped bar a ratio of 1:5) at pH 7.4. In both cases, HNE activity after carrier application is presented in relation to the activity obtained from untreated cell and supernatant controls which were both set to 100% (control, white striped bar). Controls which were taken at 21 h in parallel to the experiment show already less HNE activity in contrast to cells immediately stimulated after isolation (data not shown).

Compared to the control, the application of a 1:1 ratio to supernatant decreases HNE activity to only 85.8 ± 1.1% of the control. In contrast, the carrier application with a 1:5 ratio causes an activity to decrease to 54.8 ± 2.8%. In relation to the results obtained from cell/carrier co-incubation (filled bars) and independent of time-dependent HNE activity loss and HNE−biopolymer interaction, at both cell/carrier ratios in supernatant, a less inhibitory effect could be observed, suggesting that indeed an intracellular effect plays an important role in HNE inhibition.

In contrast to uptake experiments where carriers are exposed to acidic phagolysosomal conditions, here they are exposed to the PBS pH-neutral supernatant of stimulated PMNs. It was assumed that better extracellular multilayer stability caused the reduced inhibitory effect. First, neutral pH would stabilize the negative charge of AT and, therefore, the presence as constituent of the multilayers. Second, alterations in pH influences enzyme activities[45,51] as well as multilayer interaction. Subsequently, the multilayers will be decomposed more slowly (according to Figure 2), and multilayer-immobilized AT may not sufficiently contribute to HNE inhibition. In Rathmann *et al.*,[33] an increasing multilayer decomposition depending on decreasing pH value was described, thus supporting our assumption.

Thus, intracellular HNE inhibition at low pH seems to be more effective due to the efficient phagolysosomal multilayer decomposition and the subsequent AT release in spite of a generally reduced activity of both HNE and AT. This information also supports the results obtained from Figures 3 and 4. Nevertheless, also an increasing carrier/cell ratio results in a more effective extracellular HNE inhibition.

In summary, several concurrent processes contribute to HNE/AT interaction which therefore have to be considered. AT carriers will undergo an uptake and processing within PMNs as well as an extracellular processing, both following a different chronological sequence. Here, AT and the biopolymers PRM and DXS contribute to HNE inhibition and immobilization. In parallel to carrier processing, the cells redistribute HNE by its permanent release into the extracellular space due to ongoing stimulation.

It is also of note that in those investigations the aspect of membrane-bound HNE was not considered. A huge amount of HNE will not be freely released into the extracellular space but remains attached to the outer PMN membrane.[45] However, due to sterical hindrance, the AT-functionalized carriers are not supposed to inhibit this fraction of HNE, although microcarrier-released

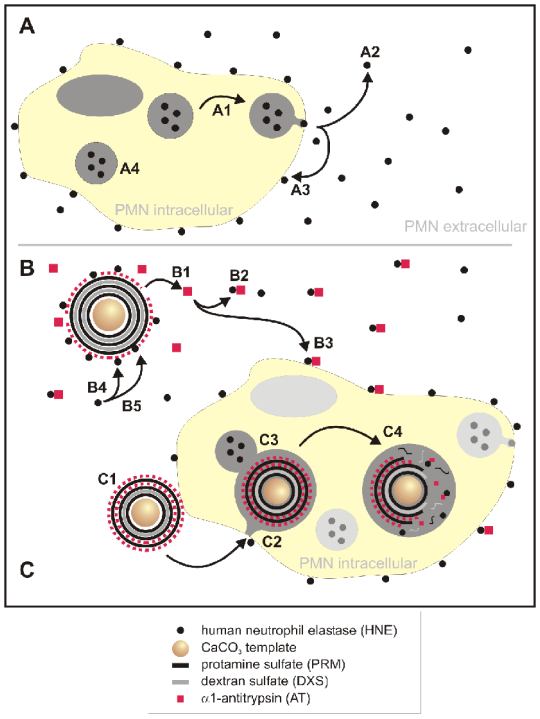


**Figure 8. Schematic presentation showing the most important processes of the complex HNE inhibition by AT-functionalized microcarriers in intra- and extracellular space of PMNs.**

AT may contribute to an inhibition. Furthermore, a possible fate of the carriers, such as by exocytosis or core degradation, was not considered. Due to the short PMN lifetime, carrier loss seems to play no significant role, but considering the complex processing of PMNs including carrier uptake and cell stimulation, apoptosis and clearance of the cells by macrophages—together with their incorporated carriers—the carriers will be finally removed from the inflamed tissue.

Nevertheless, further investigations should focus on biopolymer capsules with improved biocompatibility. Since calcium is an important second messenger and subsequently plays an activating role in most cells, the removal of the core material may enhance the biocompatibility of AT carriers in PMNs.

**AT Carrier Processing.** The AT carrier processing by PMNs within 24 h is summarized in Figure 8. Figure 8A demonstrates the general extra- and intracellular HNE distribution of PMNs in inflammatory tissue. It shows the release of the content of PMN primary granules into the extracellular space (A1) caused by stimulation. There, HNE is freely available (A2) or remains bound to the outer PMN membrane (A3). Other azurophilic granules remain within the cell (A4).

The application of AT-functionalized carriers results in an interaction with PMNs (Figure 8B,C). Hereby, the AT carriers may undergo two different processes: They may remain within the extracellular space (B) exposed to extracellular proteins and the cells secreted highly reactive substances (as HNE) or will be phagocytosed by PMNs (C).

AT surface-functionalized carriers, localized in the extracellular space (B), may contribute to the inhibition of already released HNE. Here, two options are possible: With increasing co-incubation time, AT will be partially released from the multilayers (B1, see also Figure 2) and can interact with free (B2) or in parts with membrane-bound HNE (B3) by the direct forming of stable inhibition complexes. AT/HNE complexation at the carrier surface (B4) may also be possible. Otherwise, HNE can be immobilized by interacting with the multilayer components PRM and DXS (B5), as shown in Figure 5.

In parallel, carriers adhere at the PMN surface (C1) and undergo a phagosomal uptake within 2−4 h (C2). Inside PMNs, the carrier-containing phagosome fuses with lysosomes and azurophilic granules to phagolysosomes (C3). After acidification, degradation processes may lead to multilayer decomposition and a subsequent AT release. Subsequently, AT can interact directly with HNE, resulting in a time-dependent HNE inhibition during the next 21 h (C4). Nevertheless, the multilayers or core material may contribute to the HNE inhibition as discussed for HNE inhibition in extracellular space.

In summary, microcarriers coated with biocompatible and biodegradable polymers as well as the HNE inhibitor AT facilitate both the concomitant inhibition of HNE inside and outside the cell. For combined extra- and intracellular treatment, only low amounts of microcarriers are necessary for an optimal treatment. Here, the advantages of this LbL-coated microcarrier transport system can be highlighted as transport and release of a clearly defined AT amount within PMNs in order to rebalance significantly increased HNE activity in chronic inflamed tissues.

## CONCLUSION

The application of LbL-coated colloidal microcarriers in drug delivery offers many advantages in contrast to currently used methods based on their modular and multifunctional construction principle. Especially, for the medical treatment of chronic processes, such as rheumatoid arthritis, the usage of such carriers seems to be promising.

This study is focused on inhibition of HNE, a highly reactive molecule involved in the progress of inflammation, by its natural inhibitor AT. The simultaneous HNE inhibition by carrier-transported AT outside and inside the cell improves the achieved effect and provides successful drug application.

Hereby, the microcarriers can be designed for dual AT transport by assembling AT within the multilayers: (1) AT can be coated as the outermost layer to inhibit already released HNE, and (2) AT can be integrated into the multilayers into several layer depths to undergo a time-delayed release within PMN after uptake. Both strategies are shown in our investigations.

In our approach, an AT loss of 1/3 (3 layers AT) or 1/2 (1 outermost layer AT) was observed when carriers

where stored in full medium for 4 h. According to cell/carrier interactions and an uptake time span of 2–4 h,[33] a 4 h storage time in full medium was chosen. To test the efficacy of the carrier system in the PMN application, we used one AT layer assembled onto the carrier surface. Already after short incubation, a slight HNE inhibitory effect was detectable but required an enormous numbers of carriers related to cell number. In contrast, PMN/AT carrier interaction for 21 h provoked high inhibitory effects; for example, a cell/carrier ratio of 1:5 already reduced HNE activity to 13%. It has to be noticed that both the carrier-transported AT as well as the biopolymer multilayers contributed to HNE inhibition. Assuming an efficient AT/HNE interaction of only free molecules, the AT layer has been decomposed, releasing the active agents into the phagolysosomes of the PMNs.

This assumption is also supported by the less inhibitory effect of AT toward HNE by incubating the carriers with the supernatant of stimulated PMNs at an extracellular pH of about 7.4. In this case, neutral pH, changed activity, and substrate conditions may delay the multilayer degradation and, therefore, the AT release.

In summary, we have shown that LbL-coated colloidal microcarriers offer a good opportunity to rebalance the HNE–AT concentration. In our approach, especially the simultaneous application of defined amounts of AT in the intra- and extracellular space represents a new concept in drug application for the therapeutic treatment of chronic inflammation—potentially allowing improved efficacy to current medication. This concept of local drug transport and release can be expanded regarding a variety of applications. Recent investigations using functionalized microcarriers study the treatment of cancer cells or vaccine transportation,[9,52] which may also represent interesting targets for defined and delayed drug application as shown in this work. Thus, our very specific design may show the potential of LbL carriers especially in complex applications.

## MATERIALS AND METHODS

**Preparation of $CaCO_3$ Microparticles.** $CaCO_3$ particles with $5 \pm 1$ $\mu$m diameter were prepared by rapid mixing of equal volumes of 0.33 M $CaCl_2$ and 0.33 M $Na_2CO_3$ (both Sigma-Aldrich, Germany) solutions followed by a sedimentation step as described before.[53] Afterward, the particles were washed five times in double distilled water and subsequently coated with polyelectrolyte multilayers.

**LbL Coating of $CaCO_3$ Particles.** The multilayers consisting of oppositely charged biocompatible and biodegradable polyelectrolytes protamine sulfate salt from herring (PRM, MW 4 kDa; Sigma-Aldrich, Germany) and dextran sulfate sodium salt (DXS, MW 40 kDa; INC Biochemicals, USA) were performed by alternating adsorption of initially five layers PRM and DXS. Both PRM and DXS were dissolved at a concentration of 4 mg/mL in 0.1 M sodium chloride (NaCl; Sigma-Aldrich, Germany) solution. After particle incubation for 10 min under rapid shaking at room temperature, the carriers were centrifuged and three times washed in 0.1 M NaCl solution to remove unbound polyelectrolytes.

Two experimental approaches were performed. First, up to three α1-antitrypsin (AT, 54 kDa; Sigma-Aldrich, Germany) layers were assembled onto the PRM/DXS basis multilayers each spaced with one layer of PRM following the scheme $CaCO_3$|PRM/DXS/PRM/DXS/PRM/AT/PRM/AT/PRM/AT. Second, inhibition experiments with commercially available HNE as well as released HNE from stimulated PMNs both incubated with free AT and microcarrier-transported AT were carried out. Here, only one outermost AT layer ($CaCO_3$|[PRM/DXS]$_2$PRM/AT) was used. For AT assembling, the carriers were 30 min incubated with AT dissolved in borate buffer (50 mM sodium borate, 0.2 M NaCl, pH 8.5) at a concentration of 4 mg/mL and 15 °C followed by three washing steps with 0.1 M NaCl solution.

Stability experiments were performed after carrier storage in 0.1 M NaCl solution or Dulbecco's modified Eagle medium (DMEM; PAA, Austria) containing 5% fetal calf serum (FCS; PAA, Austria).

**Labeling of AT and HNE.** To establish AT as a multilayer constituent, the protein was labeled with fluorescein isothiocyanate (FITC) according to the manufacturer's instruction (Pierce FITC Antibody Labeling Kit, Fisher Scientific GmbH, Germany). Briefly, 500 $\mu$L of AT (4 mg/mL, borate buffer pH 8.5) was incubated with FITC reagent for 60 min at room temperature. The unbound FITC was separated by gel filtration using two centrifuge columns. The label degree and AT concentration were calculated according to absorption at 280 and 495 nm. Aliquots of labeled AT were then stored at −20 °C until usage.

HNE adsorption onto the outermost AT layer of the carriers was determined by labeled HNE. HNE was labeled with NHS-Rhodamine according to the manufacturer's instruction (Pierce NHS-Rhodamine Antibody Labeling Kit, Fisher Scientific GmbH, Germany). Twenty micrograms of HNE (1 mg/mL in 50 mM Na-acetate and 200 mM NaCl) was dissolved in 180 $\mu$L of PBS (containing 50 mM borate buffer) and incubated with NHS-Rhodamine for 60 min at room temperature. Two centrifuge columns were applied to remove the unbound dye by gel filtration. The samples were used immediately for experiments.

**HNE Adsorption at Microcarrier Surfaces.** Microcarriers were prepared and coated with PRM, DXS, and AT. After each coating step, $5 \times 10^6$ carriers were separated and stored under constant shaking for further usage. Carriers with one layer (PRM), four layers (PRM and DXS, DXS surface), five layers (PRM and DXS, PRM surface), and six layers (PRM, DXS, and AT, AT- surface) were incubated in 100 $\mu$L of PBS with 68 nM HNE for 2 h in a 96-well plate. The carriers were then centrifuged and resuspended in 0.1 M NaCl and investigated by CLSM.

**Microcarrier Interaction with Commercially Available HNE.** *In vitro* experiments were carried out in 96 well-plates (100 $\mu$L). As control, 100 mM Tris (Sigma-Aldrich, Germany, pH 7.4), 68 nM HNE (Merck KGaA, stock solution 34 $\mu$M in 50 mM Na-acetate and 200 mM NaCl, pH 5.5, diluted in Tris pH 7.5), and 1 mM HNE specific substrate MeOSuc-Ala-Ala-Pro-Val-*p*-nitroanilide (Sigma-Aldrich, Germany, 50 mM stock solution in DMSO, diluted in Tris pH 8) were used to allow the spectrophotometric detection of the HNE activity by direct correlation with generated yellow *p*-nitroanilide.[54] The applied HNE concentration corresponds to HNE of $3 \times 10^5$ cells.[55,56] Then, $3 \times 10^5$ (cell/carrier ratio 1:1), $15 \times 10^5$ (cell/carrier ratio 1:5), or $30 \times 10^5$ (cell/carrier ratio 1:10) AT-functionalized carriers were added to the mixture.

The activity of immobilized AT was compared to approaches using free AT (0.19 to 2.86 $\mu$M) instead of microcarrier application (data not shown) realizing a gradual HNE inactivation.

**Isolation of Polymorphonuclear Leukocytes (PMNs).** PMNs were isolated from human whole blood of healthy donors (obtained from blood bank) as described before.[57] In order to remove erythrocytes, 10 mL of heparin-treated blood (Merck KGaA, Germany, 100U in 1 mL) was incubated with 1 mL of dextran (70 kDa, Sigma-Aldrich, Germany, 20% in 0.9% NaCl solution). After density gradient centrifugation (400*g*, 4 °C for 25 min, Histopaque,

1.077 g/mL, Sigma-Aldrich, Germany), the remaining erythrocytes were removed by hypotonic lysis (30 s). The PMN pellet was resuspended in Hank's buffered salt solution without $CaCl_2$ ($HBSS^-$, Sigma-Aldrich, Germany).

**Microcarrier Interaction with Released Elastase and Their Co-incubation with PMNs.** According to microcarrier interaction with commercially available HNE, $3 \times 10^5$ cells (in 60 $\mu$L HBSS with $CaCl_2$ ($HBSS^+$; Sigma-Aldrich, Germany)) were stimulated by means of $10^{-7}$ M phorbol 12-myristate 13-acetate (PMA; Sigma-Aldrich, Germany, $10^{-2}$ M stock solution in DMSO, diluted in $HBSS^+$) for 30 min at 37 °C. Then, supernatant was carefully collected into 1.5 mL tubes and centrifuged twice: The first centrifugation step at 500 rcf for 5 min was chosen for a gentle removal of the cells without further disruption and, therefore, without additional HNE release. The second step at 2500 rcf for 1 min was performed in order to achieve a complete removal of potential remaining cell debris. The samples were buffered with 30 $\mu$L of PBS (pH 7.4) and citrate phosphate buffer (pH 5), respectively. After adding the carriers, 10 $\mu$L of substrate was added to the solution for a final concentration of 1 mM.

Cell/carrier experiments ($10^6$ PMNs per well) were carried out in 48-well plates. Those plates were used to ensure a homogeneous cell distribution. After centrifugation, $10^6$ PMNs per well were resuspended in $HBSS^+$. Although there can be a slight cell stimulation due to the $Ca^{2+}$-containing buffer, this step was necessary to avoid a buffer exchange after cell/carrier co-incubation. According to experimental conditions, $10^6$ (cell/carrier ratio 1:1), $5 \times 10^6$ (cell/carrier ratio 1:5), or $10 \times 10^6$ (cell/carrier ratio 1:10) microcarriers were resuspended in 10 $\mu$L of PBS and added to the cells for co-incubation (5 and 21 h at 37 °C). PMNs without carrier co-incubation served as the control taken according to the co-incubation time spans.

For detection of extracellularly released HNE, PMNs were stimulated by means of PMA for 30 min at 37 °C. Then, supernatant was carefully collected into 1.5 mL tubes as described above. Afterward, the samples were buffered with 90 $\mu$L of PBS (pH 7.4), and the supernatant of each well was photometrically investigated. Therefore, 33 $\mu$L of specific HNE substrate was added to each tube for 2 h with a final concentration of 1 mM.

As positive references, the HNE release was induced immediately after PMN isolation as well as after the experimental incubation time without any microcarrier incubation.

In order to detect total HNE activity, consisting of the extracellular released as well as already membrane-bound HNE, the protocol was modified. After co-incubation of carriers and PMNs, the samples were directly incubated with substrate for 2 h. Afterward, the supernatant was collected and analyzed according to the protocol.

**Flow Cytometry (FCM).** FCM (FACSCalibur, BD Biosciences) was used for the determination of the AT amount assembled onto the PRM/DXS multilayers as well as for the detection of surface-bound HNE. The geometric mean FITC fluorescence intensity of labeled AT as well as RITC intensity of labeled HNE bound to carriers was detected after a laser excitation of $10^4$ carriers at 488 nm using the 530/30 nm band-pass filter (channel FL1) and 585/42 nm band-pass filter (channel FL2), respectively. FITC intensities were correlated with intensities of FITC-labeled beads (SPHERO FITC calibration particle kit, G. Kisker GbR, Germany) which are equipped with defined numbers of FITC molecules ($0.24 \pm 0.02$). This allows the determination of bound AT.

**Confocal Laser Scanning Microscopy (CLSM).** Confocal laser scanning fluorescence microscopy (Zeiss, LSM 510 META, Germany) was applied to visualize the homogeneous distribution of AT as multilayer constituent and HNE adsorption. A laser excitation of 488 nm (argon laser) was used to detect FITC fluorescence of labeled AT by a band-pass filter of 505−525 nm, and NHS-Rhodamine was excited at 543 nm (HeNe laser) and detected with a band-pass filter of 560−615 nm.

**Spectrophotometric Detection.** AT label degree and concentration were calculated from absorption values at 280 and 495 nm determined by a NanoDrop spectrophotometer (ND1000, Thermo Scientific).

HNE activity was detected photometrically by a Multimode plate reader (Tecan Infinite M200) using a 96-well plate. One hundred microliters of each sample was added, and absorption was detected at 410 nm.

*Conflict of Interest:* The authors declare no competing financial interest.

*Acknowledgment.* The authors would like to thank Scott A. Irvine for valuable comments and proofreading. The work presented in this paper was made possible by funding from German Research Foundation (DFG, RE 2681/2-1), the German Federal Ministry of Education and Research (BMBF, PtJ-Bio, 0313909), the European Union and the Free State of Saxony and was supported by the DFG graduate school 185 "Leipzig School of Natural Sciences—Building with Molecules and Nano-objects" (BuildMoNa).

## REFERENCES AND NOTES

1. Chung, C. P.; Avalos, I.; Raggi, P.; Stein, C. M. Atherosclerosis and Inflammation: Insights from Rheumatoid Arthritis. *Clin. Rheumatol.* **2007**, *26*, 1228–1233.
2. Doan, T.; Massarotti, E. Rheumatoid Arthritis: An Overview of New and Emerging Therapies. *J. Clin. Pharmacol.* **2005**, *45*, 751–762.
3. Peyratout, C. S.; Dahne, L. Tailor-Made Polyelectrolyte Microcapsules: From Multilayers to Smart Containers. *Angew. Chem., Int. Ed* **2004**, *43*, 3762–3783.
4. Donath, E.; Sukhorukov, G. B.; Caruso, F.; Davis, S. A.; Mohwald, H. Novel Hollow Polymer Shells by Colloid-Templated Assembly of Polyelectrolytes. *Angew. Chem., Int. Ed* **1998**, *37*, 2202–2205.
5. Yashchenok, A. M.; Delcea, M.; Videnova, K.; Jares-Erijman, E. A.; Jovin, T. M.; Konrad, M.; Mohwald, H.; Skirtach, A. G. Enzyme Reaction in the Pores of $CaCO_3$ Particles upon Ultrasound Disruption of Attached Substrate-Filled Liposomes. *Angew. Chem., Int. Ed* **2010**, *49*, 8116–8120.
6. Becker, A. L.; Johnston, A. P. R.; Caruso, F. Peptide Nucleic Acid Films and Capsules: Assembly and Enzymatic Degradation. *Macromol. Biosci.* **2010**, *10*, 488–495.
7. De Koker, S.; De Cock, L. J.; Rivera-Gil, P.; Parak, W. J.; Velty, R. A.; Vervaet, C.; Remon, J. P.; Grooten, J.; De Geest, B. G. Polymeric Multilayer Capsules Delivering Biotherapeutics. *Adv. Drug Delivery Rev.* **2011**, *63*, 748–761.
8. Vergaro, V.; Scarlino, F.; Bellomo, C.; Rinaldi, R.; Vergara, D.; Maffia, M.; Baldassarre, F.; Giannelli, G.; Zhang, X. C.; Lvov, Y. M.; *et al.* Drug-Loaded Polyelectrolyte Microcapsules for Sustained Targeting of Cancer Cells. *Adv. Drug Delivery Rev.* **2011**, *63*, 847–863.
9. De Geest, B. G.; Willart, M. A.; Hammad, H.; Lambrecht, B. N.; Pollard, C.; Bogaert, P.; De Filette, M.; Saelens, X.; Vervaet, C.; Remon, J. P.; *et al.* Polymeric Multilayer Capsule-Mediated Vaccination Induces Protective Immunity Against Cancer and Viral Infection. *ACS Nano* **2012**, *6*, 2136–2149.
10. Reibetanz, U.; Claus, C.; Typlt, E.; Hofmann, J.; Donath, E. Defoliation and Plasmid Delivery with Layer-by-Layer Coated Colloids. *Macromol. Biosci.* **2006**, *6*, 153–160.
11. Reibetanz, U.; Halozan, D.; Brumen, M.; Donath, E. Flow Cytometry of HEK 293T Cells Interacting with Polyelectrolyte Multilayer Capsules Containing Fluorescein-Labeled Poly(acrylic acid) as a pH Sensor. *Biomacromolecules* **2007**, *8*, 1927–1933.
12. Semmling, M.; Kreft, O.; Javier, A. M.; Sukhorukov, G. B.; Kas, J.; Parak, W. J. A Novel Flow-Cytometry-Based Assay for Cellular Uptake Studies of Polyelectrolyte Microcapsules. *Small* **2008**, *4*, 1763–1768.
13. Rivera-Gil, P.; De Koker, S.; De Geest, B. G.; Parak, W. J. Intracellular Processing of Proteins Mediated by Biodegradable Polyelectrolyte Capsules. *Nano Lett.* **2009**, *9*, 4398–4402.
14. Wang, Z. J.; Qian, L.; Wang, X. L.; Zhu, H.; Yang, F.; Yang, X. R. Hollow DNA/PLL Microcapsules with Tunable Degradation Property as Efficient Dual Drug Delivery Vehicles by α-Chymotrypsin Degradation. *Colloids Surf., A* **2009**, *332*, 164–171.
15. Yu, A. M.; Gentle, I. R.; Lu, G. Q. Biocompatible Polypeptide Microcapsules *via* Templating Mesoporous Silica Spheres. *J. Colloid Interface Sci.* **2009**, *333*, 341–345.

16. De Geest, B. G.; Sanders, N. N.; Sukhorukov, G. B.; Demeester, J.; De Smedt, S. C. Release Mechanisms for Polyelectrolyte Capsules. *Chem. Soc. Rev* **2007**, *36*, 636–649.
17. Matsusaki, M.; Akashi, M. Functional Multilayered Capsules for Targeting and Local Drug Delivery. *Expert Opin. Drug Delivery* **2009**, *6*, 1207–1217.
18. De Geest, B. G.; Sukhorukov, G. B.; Mohwald, H. The Pros and Cons of Polyelectrolyte Capsules in Drug Delivery. *Expert Opin. Drug Delivery* **2009**, *6*, 613–624.
19. Skirtach, A. G.; Yashchenok, A. M.; Mohwald, H. Encapsulation, Release and Applications of LbL Polyelectrolyte Multilayer Capsules. *Chem. Commun.* **2011**, *47*, 12736–12746.
20. Sato, K.; Yoshida, K.; Takahashi, S.; Anzai, J. I. pH- and Sugar-Sensitive Layer-by-Layer Films and Microcapsules for Drug Delivery. *Adv. Drug Delivery Rev.* **2011**, *63*, 809–821.
21. Qi, W.; Yan, X. H.; Fei, J. B.; Wang, A. H.; Cui, Y.; Li, J. B. Triggered Release of Insulin from Glucose-Sensitive Enzyme Multilayer Shells. *Biomaterials* **2009**, *30*, 2799–2806.
22. Skirtach, A. G.; Javier, A. M.; Kreft, O.; Kohler, K.; Alberola, A. P.; Mohwald, H.; Parak, W. J.; Sukhorukov, G. B. Laser-Induced Release of Encapsulated Materials Inside Living Cells. *Angew. Chem., Int. Ed* **2006**, *45*, 4612–4617.
23. Javier, A. M.; del Pino, P.; Bedard, M. F.; Ho, D.; Skirtach, A. G.; Sukhorukov, G. B.; Plank, C.; Parak, W. J. Photoactivated Release of Cargo from the Cavity of Polyelectrolyte Capsules to the Cytosol of Cells. *Langmuir* **2008**, *24*, 12517–12520.
24. De Geest, B. G.; Skirtach, A. G.; Mamedov, A. A.; Antipov, A. A.; Kotov, N. A.; De Smedt, S. C.; Sukhorukov, G. B. Ultrasound-Triggered Release from Multilayered Capsules. *Small* **2007**, *3*, 804–808.
25. Reibetanz, U.; Lessig, J.; Hoyer, J.; Neundorf, I. Surface Functionalized Colloidal Microparticles for Fast Endocytotic Cell Uptake. *Adv. Eng. Mater.* **2010**, *12*, B488–B495.
26. Cortez, C.; Tomaskovic-Crook, E.; Johnston, A. P. R.; Scott, A. M.; Nice, E. C.; Heath, J. K.; Caruso, F. Influence of Size, Surface, Cell Line, and Kinetic Properties on the Specific Binding of A33 Antigen-Targeted Multilayered Particles and Capsules to Colorectal Cancer Cells. *ACS Nano* **2007**, *1*, 93–102.
27. De Koker, S.; De Geest, B. G.; Cuvelier, C.; Ferdinande, L.; Deckers, W.; Hennink, W. E.; De Smedt, S.; Mertens, N. *In Vivo* Cellular Uptake, Degradation, and Biocompatibility of Polyelectrolyte Microcapsules. *Adv. Funct. Mater.* **2007**, *17*, 3754–3763.
28. Baggolini, M.; Bretz, U.; Dewald, B.; Feigenson, M. E. Polymorphonuclear Leukocyte. *Agents Actions* **1978**, *8*, 3–10.
29. Webb, P. R.; Wang, K. Q.; Scheel-Toellner, D.; Pongracz, J.; Salmon, M.; Lord, J. M. Regulation of Neutrophil Apoptosis: A Role for Protein Kinase C and Phosphatidylinositol-3-Kinase. *Apoptosis* **2000**, *5*, 451–458.
30. Borregaard, N.; Cowland, J. B. Granules of the Human Neutrophilic Polymorphonuclear Leukocyte. *Blood* **1997**, *89*, 3503–3521.
31. Javier, A. M.; Kreft, O.; Semmling, M.; Kempter, S.; Skirtach, A. G.; Bruns, O. T.; del Pino, P.; Bedard, M. F.; Raedler, J.; Kaes, J.; *et al.* Uptake of Colloidal Polyelectrolyte-Coated Particles and Polyelectrolyte Multilayer Capsules by Living Cells. *Adv. Mater.* **2008**, *20*, 4281–4287.
32. Lessig, J.; Neu, B.; Reibetanz, U. Influence of Layer-by-Layer (LbL) Assembled $CaCO_3$-Carriers on Macrophage Signaling Cascades. *Biomacromolecules* **2011**, *12*, 105–115.
33. Rathmann, S.; Schönberg, M.; Leßig, J.; Reibetanz, U. Interaction, Uptake and Processing of LbL-Coated Microcarriers by PMNs. *Cytometry, Part A* **2011**, *79A*, 979–989.
34. Reh, G.; Nerli, B.; Pico, G. Isolation of α-1-Antitrypsin in Aqueous Biphasic Systems from Human Plasma by Partitioning of Polyethyleneglycol-Phosphate. *J. Chromatogr.* **2002**, *780*, 389–396.
35. De Temmerman, M. L.; Demeester, J.; De Vos, F.; De Smedt, S. C. Encapsulation Performance of Layer-by-Layer Microcapsules for Proteins. *Biomacromolecules* **2011**, *12*, 1283–1289.
36. Hiller, S.; Leporatti, S.; Schnackel, A.; Typlt, E.; Donath, E. Protamine Assembled in Multilayers on Colloidal Particles Can Be Exchanged and Released. *Biomacromolecules* **2004**, *5*, 1580–1587.
37. Caruso, F.; Schuler, C. Enzyme Multilayers on Colloid Particles: Assembly, Stability, and Enzymatic Activity. *Langmuir* **2000**, *16*, 9595–9603.
38. Lentacker, I.; De Geest, B. G.; Vandenbroucke, R. E.; Peeters, L.; Demeester, J.; De Smedt, S. C.; Sanders, N. N. Ultrasound-Responsive Polymer-Coated Microbubbles That Bind and Protect DNA. *Langmuir* **2006**, *22*, 7273–7278.
39. De Geest, B. G.; Vandenbroucke, R. E.; Guenther, A. M.; Sukhorukov, G. B.; Hennink, W. E.; Sanders, N. N.; Demeester, J.; De Smedt, S. C. Intracellularly Degradable Polyelectrolyte Microcapsules. *Adv. Mater.* **2006**, *18*, 1005–1009.
40. Haslett, C. Granulocyte Apoptosis and Inflammatory Disease. *Br. Med. Bull.* **1997**, *53*, 669–683.
41. Flemmig, J.; Lessig, J.; Reibetanz, U.; Dautel, P.; Arnhold, J. Non-vital Polymorphonuclear Leukocytes Express Myeloperoxidase on Their Surface. *Cell. Physiol. Biochem.* **2008**, *21*, 287–296.
42. Schönberg, M.; Reibetanz, U.; Rathmann, S.; Lessig, J. Maintenance of α1-Antitrypsin Activity by Means of Co-application of Hypochlorous Acid-Scavengers *in Vitro* and in the Supernatant of Polymorphonuclear Leukocytes—As a Basis for a New Drug Delivery Approach. *Biomatter* **2012**, *2*, 1–13.
43. Jacques, Y. V.; Bainton, D. F. Changes in pH within Phagocytic Vacuoles of Human Neutrophils and Monocytes. *Lab. Invest.* **1978**, *39*, 179–185.
44. Lehrer, R. I.; Ganz, T. Antimicrobial Polypeptides of Human Neutrophils. *Blood* **1990**, *76*, 2169–2181.
45. Owen, C. A.; Campbell, E. J. The Cell Biology of Leukocyte-Mediated Proteolysis. *J. Leukocyte Biol.* **1999**, *65*, 137–150.
46. Hoffmann, J. J. M. L.; Vandenbroek, W. G. M.; Jansen, A. P. Automated Determination of Antitrypsin Activity of Serum. *Clin. Chim. Acta* **1976**, *71*, 251–259.
47. Devlin, G. L.; Chow, M. K. M.; Howlett, G. J.; Bottomley, S. P. Acid Denaturation of α(1)-Antitrypsin: Characterization of a Novel Mechanism of Serpin Polymerization. *J. Mol. Biol.* **2002**, *324*, 859–870.
48. Dafforn, T. R.; Mahadeva, R.; Elliott, P. R.; Sivasothy, P.; Lomas, D. A. A Kinetic Mechanism for the Polymerization of α(1)-Antitrypsin. *J. Mol. Biol.* **1999**, *274*, 9548–9555.
49. Zhang, Z.; Farrell, A. J.; Blake, D. R.; Chidwick, K.; Winyard, P. G. Inactivation of Synovial-Fluid α-1-Antitrypsin by Exercise of the Inflamed Rheumatic Joint. *FEBS Lett.* **1993**, *321*, 274–278.
50. Korkmaz, B.; Moreau, T.; Gauthier, F. Neutrophil Elastase, Proteinase 3 and Cathepsin G: Physicochemical Properties, Activity and Physiopathological Functions. *Biochimie* **2008**, *90*, 227–242.
51. Klebanoff, S. J. Antimicrobial Mechanisms in Neutrophilic Polymorphonuclear Leukocytes. *Semin. Hematol.* **1975**, *12*, 117–142.
52. De Koker, S.; Lambrecht, B. N.; Willart, M. A.; van Kooyk, Y.; Grooten, J.; Vervaet, C.; Remon, J. P.; De Geest, B. G. Designing Polymeric Particles for Antigen Delivery. *Chem. Soc. Rev.* **2011**, *40*, 320–339.
53. Volodkin, D. V.; Larionova, N. I.; Sukhorukov, G. B. Protein Encapsulation *via* Porous $CaCO_3$ Microparticles Templating. *Biomacromolecules* **2004**, *5*, 1962–1972.
54. Cook, L.; Burdon, J. G. W.; Brenton, S.; Knight, K. R.; Janus, E. D. Kinetic Characterisation of α-1-Antitrypsin F as an Inhibitor of Human Neutrophil Elastase. *Pathology* **1996**, *28*, 242–247.
55. Meyer-Hoffert, U. Neutrophil-Derived Serine Proteases Modulate Innate Immune Responses. *Front. Biosci.* **2009**, *14*, 3409–3418.
56. Dewald, B.; Rindlerludwig, R.; Bretz, U.; Baggolini, M. Subcellular-Localization and Heterogeneity of Neutral Proteases in Neutrophilic Polymorphonuclear Leukocytes. *J. Exp. Med.* **1975**, *141*, 709–723.
57. Boyum, A. Separation of Leukocytes from Blood and Bone Marrow. Introduction. *Scand. J. Clin. Lab. Inv. Suppl.* **1968**, *97*, 7.